Prepared for submission to JHEP

# LHCb anomaly in $B \to K^*\mu^+\mu^-$ optimised observables and potential of $Z'$ Model

**Ishtiaq Ahmed and Abdur Rehman**

*National Centre for Physics, Quaid-i-Azam University Campus, Islamabad 45320, Pakistan*

*E-mail:* ishtiaq@ncp.edu.pk; abdur.rehman@ncp.edu.pk

Abstract: The measurements of LHCb with present energies found some discrepancies in $b \to s\ell^+\ell^-$ FCNC transitions over the last few years. In 2013, LHCb announced very famous anomalies in the angular observables of $B \to K^*\mu^+\mu^-$, particularly in $P_5'$, in low dimuon mass region. Recently, these anomalies are confirmed by LHCb, Belle, CMS and ATLAS. To accommodate these anomalies through QCD corrections in the form factors at next to leading order and through charm loop effects are disfavored. As the direct evidence of physics beyond-the-SM is absent so far, therefore, these anomalies are being interpreted as indirect hint of new physics. In this context, we study the implication of non universal family of $Z'$ model to the form factor independent angular observables $P_{1,2,3}$, $P'_{4,5,6}$ and newly proposed lepton flavor universality violation observables, $Q_{4,5}$, in $B \to K^*(\to K\pi)\mu^+\mu^-$ decay channel in the low dimuon mass region. To see variation in the values of these observables from their standard model values, we have chosen the different scenarios of the $Z'$ model. It is found that these angular observables are sensitive to the values of the parameters of $Z'$ model. We have also found that with the present parametric space of $Z'$ model, the $P_5'$-anomaly could be accommodated. However, more statistics on the anomalies in the angular observables, if persist, are helpful to put constraint on the parametric space of considered model and, in general, helpful to reveal the nature of new physics.

Keywords: $B$-physics, angular observables, beyond standard model

arXiv:1703.09627v1 [hep-ph] 28 Mar 2017

## Contents


**1 Introduction** **1**

**2 Formulation for the Analysis** **3**
2.1 Matrix Elements and Form Factors 3
2.2 Expressions of the Angular Observables 5

**3 Results and Discussion** **7**
3.1 $P$-observables in different bin size 7
3.2 $P$-observables in $s \in [1.0, 6.0]$ GeV$^2$ 10
3.3 $Q_{4,5}$ for $s \in [1.0, 6.0]$ GeV$^2$ 12

**4 Conclusion** **12**

**A Input parameters** **14**

**B NLO contributions in the low dilepton mass limit** **14**


## 1 Introduction

In flavor physics, study of rare $B$ meson decays provide us a powerful tool to test standard model (SM) at loop level as well as to search possible new physics (NP). To search NP in rare decays of B-meson demands to focus on these observables which contain minimum hadronic uncertainties such that they can be predicted precisely in the SM and are available at current colliders. As in the exclusive rare B meson decays, the long distance physics encapsulated in the transition matrix elements that can be parameterized in terms of form factors. The main source of hadronic uncertainties comes from these form factors which are non-perturbative quantities and are difficult to compute and may preclude the signature of any possible NP. From this point of view, among all rare decays, the four body decay channel, $B \to K^*(\to K\pi)\mu^+\mu^-$, have a special interest in literature due to the fact that it gives a large variety of angular observables which are free from hadronic uncertainties and are available experimentally, for instance, optimal observables that are denoted in the literature as $P_i$ $(i = 1, 2, 3)$ and $P_i'$ $(i = 4, 5, 6)$. The comparison between the theoretical predictions of these kind of observables in and beyond the SM with the experimental data could be helpful to clear some smog on beyond-SM physics.

The primed observables, introduced in ref. [1] and are free of form-factor uncertainties [2]. From experimental point of view, recently, LHCb analysis on these angular observables for $B \to K^*(\to K\pi)\mu^+\mu^-$ indicates notably deviation from SM expectations, mainly $3.7\sigma$ discrepancy with data set of 1 fb$^{-1}$ in the $P_5'$ observable, at large recoil, in the $s \in [4.30, 8.68]$

[3], where $s$ is the dimuon invariant mass squared, $q^2$. This discrepancy again seen at LHCb with a $3\sigma$ deviation with 3 fb$^{-1}$ luminosity, comparatively, in two shorter adjacent bins $s \in [4,6]$ [4] and $s \in [6,8]$ which is also confirmed by Belle in the larger bin $s \in [4,8]$ [6, 7]. The very recent results from ATLAS [8] and CMS [9, 10] collaborations are presented in Moriond 2017. With these results a state of the art global analysis, performed by the authors of ref. [11], show that there is a sizable discrepancy between data and SM. In addition, LHCb also found $2.6\sigma$ deviation from the SM prediction in the ratio $R_K = \text{Br}(B \to K\mu^+\mu^-)/\text{Br}(B \to Ke^+e^-)$ [12], and $\gtrsim 2\sigma$ in the $\text{Br}(B_s \to \phi\mu^+\mu^-)$ [13]. Interestingly, all these deviations belong to the rare $B$ meson decays which is flavor changing neutral current (FCNC) transitions and at quark level it is shown as, $b \to s\ell^+\ell^-$, where $\ell^-$ denotes final state leptons. It is important to mention here that even angular observables are form factor independent (FFI) but for precise theoretical predictions of their values, one needs to incorporate the QCD corrections. There are two classes of QCD corrections contributing to $B \to$ meson transitions, namely, factorisable and non-factorisable. The factorisable means those contributions which comes through soft interaction of the spectator quarks and can be absorbed in hadronic form factors while the non-factorisable contributions arise from hard scattering of the process and do not belong to the form factors. In the present study, to determine the values of angular observables, we have incorporated both type of corrections in our numerical analysis available up to next-to-leading order (NLO) and the expressions of these contributions are given in Appendix B.

As these anomalies are slowly piled up, they received a considerable attention in the literature (see for instance [11, 14]). Regarding these anomalies, another interesting debate recently appeared in the literature, whether they emerge from unknown factorisable power corrections or from NP. As the authors of Ref. [15] claim that these anomalies cannot be accommodate by large hadronic power corrections while the authors of Ref. [16] indicated that one cannot eliminate the choice that the current anomalies are partly outcome of underrated uncertainties in the form factor calculations which arise from power corrections. However, by keeping both of these arguments, global fit analysis [11] with present data, strongly pointed out that instead of this inconclusive situation, the interpretation of anomalies through the NP is a valid option.

To alleviate these anomalies, several NP models have been put forward [17–22]. From NP point of view, an extension in the SM consider to be good and simple which is economical and alleviate most of the existing anomalies simultaneously through a common mechanism in a consistent way. In this regard, the $Z'$ model is economical due to the fact that it requires only one extra $U(1)'$ gauge symmetry associate with the neutral gauge boson, called $Z'$ with the SM gauge group. The nature of couplings of the $Z'$ boson with the quarks and leptons leads the FCNC transitions to the tree level. This feature of the model arises that NP effects comes only through the short distance Wilson coefficients which are encapsulated in the new coefficients $C_9^{\text{tot}} = C_9^{\text{SM}} + C_9^{Z'}$, $C_{10}^{\text{tot}} = C_{10}^{\text{SM}} + C_{10}^{Z'}$, while operator basis remained unchange.

In addition, several previous studies on different observables of decay $B \to K^*\mu^+\mu^-$ in which SM values deviate from their experimental measurements have already been discussed and shown a possible interpretation of these mismatch in terms of $Z'$ model [23–28].

It is natural to ask whether the $Z'$ model could explain the recently observed anomalies in the angular observables of the decay channel $B \to K^*(\to K\pi)\mu^+\mu^-$. With this motivation, in the current study, we have analyzed the optimal observables $P_{1,2,3}$ and $P'_{4,5,6}$, in the low dimuon mass region, for the $B \to K^*(\to K\pi)\mu^+\mu^-$ in the SM and in the $Z'$ models. Besides this we also calculated the violation of lepton flavor universality (LFU) observables namely, $Q_{4(5)} = P'^{\mu}_{4(5)} - P'^{e}_{4(5)}$ [29]. For numerical calculations of these observables, we have used the light cone sum rules (LCSR) values of the hadronic form factors [30] and the numerical values of $Z'$ parameters are given in Tab. (5).

This paper is organized as follows: in section 2.1, we write the effective Hamiltonian for the $b \to s\ell^+\ell^-$ transition in the SM and the modified Hamiltonian after incorporating contributions that come through the $Z'$ boson. The $B \to K^*$ matrix elements in terms of form factors and the expression of four differential decay distributions are also given in this section. Formulae for the angular observables and their analytical expressions are given in section 2.2. In section 3, we have plotted the angular observables and their average values against dimuon mass $s$ and we have given phenomenological analysis of these observables. In the last section we conclude our work. Appendix A contains the values of input parameters needed for our numerical calculations. The factorisable and non-factorisable contributions at NLO are summarized in Appendix B.

## 2 Formulation for the Analysis

### 2.1 Matrix Elements and Form Factors

In the standard model, FCNC processes occur at loop level and the amplitude of $b \to s\ell^+\ell^-$ can be written as following,

$$\mathcal{M}^{\rm SM}(b \to s\ell^+\ell^-) = -\frac{\alpha\, G_F}{2\sqrt{2}\pi} V_{tb}V_{ts}^* \Big\{ \langle K^*(p_{K^*},\epsilon)|\bar{s}\gamma^\mu Lb|B(p_B)\rangle (C_9^{\rm eff}\bar{\ell}\gamma^\mu\ell + C_{10}^{\rm SM}\bar{\ell}\gamma^\mu\gamma_5\ell) - 2m_b C_7^{\rm eff}\langle K^*(p_{K^*},\epsilon)|\bar{s}i\sigma_{\mu\nu}\frac{q^\nu}{q^2}Rb|B(p_B)\rangle\,\bar{\ell}\gamma^\mu\ell\Big\}, \tag{2.1}$$

where $L, R = (1\pm\gamma^5)$, $p_{K^*}$ and $\epsilon$ are momentum and polarization of $K^*$ meson, respectively, while $p_B$ is the momentum of $B$ meson.

In the presence of $Z'$ the FCNC transitions could occur at tree level and the Hamiltion is written in the following form (see detail in the refs. [31–34] )

$$\mathcal{H}_{\rm eff}^{Z'}(b \to s\ell^+\ell^-) = -\frac{4G_F}{\sqrt{2}} V_{tb}V_{ts}^* \Big[\Lambda_{sb}\, C_9^{Z'} O_9 + \Lambda_{sb}\, C_{10}^{Z'} O_{10}\Big], \tag{2.2}$$

$$\text{where,} \quad \Lambda_{sb} = \frac{4\pi e^{-i\phi_{sb}}}{\alpha_{em} V_{tb}V_{ts}^*}, \qquad C_9^{Z'} = |\mathcal{B}_{sb}|S_{\ell\ell}^{LR}, \qquad C_{10}^{Z'} = |\mathcal{B}_{sb}|D_{\ell\ell}^{LR},$$

$$\text{with,} \quad \mathcal{S}_{\ell\ell}^{LR} = \mathcal{B}_{\ell\ell}^{L} + \mathcal{B}_{\ell\ell}^{R}, \qquad \mathcal{D}_{\ell\ell}^{LR} = \mathcal{B}_{\ell\ell}^{L} - \mathcal{B}_{\ell\ell}^{R}. \tag{2.3}$$

The $\mathcal{B}_{sb}$ is the coupling of $Z'$ with quarks and $\mathcal{B}_{\ell\ell}^{L}$, $\mathcal{B}_{\ell\ell}^{R}$ are left and right-handed couplings fo $Z'$ with leptons. One can notice from Eq. (2.3) that in the $Z$-prime model, operator basis remains the same as in the SM and $C_9$ and $C_{10}$ get modifications while $C_7^{\rm eff}$ remains

unchanged. The total amplitude for the decay $B \to K^*\ell^+\ell^-$ is the sum of SM and $Z'$ contributions, and can be written as follows,

$$\mathcal{M}^{tot}(B \to K^*\ell^+\ell^-) = -\frac{\alpha\, G_F}{2\sqrt{2}\pi} V_{tb}V_{ts}^* \Big\{ \langle K^*(p_{K^*},\epsilon)|\bar{s}\gamma^\mu Lb|B(p_B)\rangle (C_9^{\rm tot}\bar{\ell}\gamma^\mu\ell + C_{10}^{\rm tot}\bar{\ell}\gamma^\mu\gamma_5\ell) \\ -2m_b C_7^{\rm eff}\langle K^*(p_{K^*},\epsilon)|\bar{s}i\sigma_{\mu\nu}\tfrac{q^\nu}{q^2}Rb|B(p_B)\rangle\bar{\ell}\gamma^\mu\ell\Big\}, \tag{2.4}$$

where $C_9^{\rm tot} = C_9^{\rm eff} + \Lambda_{sb}C_9^{Z'}$ and $C_{10}^{\rm tot} = C_{10}^{\rm SM} + \Lambda_{sb}C_{10}^{Z'}$.

The matrix elements of the quark operators for the decay amplitude for $B \to K^*\ell^+\ell^-$ appears in Eq. (2.4) can be written in terms of form factors as follows

$$\langle K^*(p_{K^*},\epsilon)|\bar{s}\gamma^\mu Lb|B(p_B)\rangle = -iq_\mu\frac{2m_{K^*}}{s}\epsilon^*\cdot q\Big[A_3(s) - A_0(s)\Big] - \epsilon_{\mu\nu\lambda\sigma}\epsilon^{*\nu}p_{K^*}^\lambda q^\sigma\frac{2V(s)}{(m_B+m_{K^*})} \\ +i\epsilon_\mu^*(m_B+m_{K^*})A_1(s) \mp i(p_B+p_{K^*})_\mu\epsilon^*\cdot q\frac{A_2(s)}{(m_B+m_{K^*})},$$

$$\langle K^*(p_{K^*},\epsilon)|\bar{s}i\sigma_{\mu\nu}q^\nu Rb|B(p_B)\rangle = 2\epsilon_{\mu\nu\lambda\sigma}\epsilon^{*\nu}p_{K^*}^\lambda q^\sigma\ T_1(s) + \ i\epsilon^*\cdot q\Big\{q_\mu - \frac{(p_B+p_{K^*})_\mu s}{(m_B^2-m_{K^*}^2)}\Big\}T_3(s) \\ +\ i\Big\{\epsilon_\mu^*(m_B^2-m_{K^*}^2) - (p_B+p_{K^*})_\mu\epsilon^*\cdot q\Big\}\ T_2(s), \tag{2.5}$$

where,

$$A_3(s) = \frac{m_B+m_{K^*}}{2m_{K^*}}A_1(s) - \frac{m_B-m_{K^*}}{2m_{K^*}}A_2(s)\ . \tag{2.6}$$

Here $A_{0,1,2}(s)$, $V(s)$, $T_{1,2,3}(s)$ are the form factors and contain hadronic uncertainties. At leading order by using the heavy quark limit, the QCD form factors follow the symmetry relations and can be expressed in terms of two universal form factors $\xi_\perp$ and $\xi_\parallel$ [35, 36].

$$\xi_\perp = \frac{m_B}{m_B+m_{K^*}}V, \qquad \xi_\parallel = \frac{m_B+m_{K^*}}{2E_{K^*}}A_1 - \frac{m_B-m_{K^*}}{m_B}A_2. \tag{2.7}$$

For the $s$ dependence of the universal form factors, we use the following parameterization of light cone sum rule (LCSR) approach [30].

$$V(s) = \frac{r_1}{1-s/m_R^2} + \frac{r_2}{1-s/m_{fit}^2}, \qquad A_1(s) = \frac{r_2}{1-s/m_{fit}^2}, \\ A_2(s) = \frac{r_1}{1-s/m_{fit}^2} + \frac{r_2}{(1-s/m_{fit}^2)^2}, \tag{2.8}$$

where the parameters $r_{1,2}$, $m_R^2$ and $m_{fit}^2$ are listed in Tab. (1). The uncertainty in the universal form factors $\xi_\perp$ and $\xi_\parallel$ arises from the uncertainty in the different parameters using in LCSR approach which is about 11% and 14%, respectively, as discussed in [35]. At NLO, the relations between the $T_i(s)$ where $(i = 1, 2, 3)$ and the invariant amplitudes $\mathcal{T}_{\perp,\parallel}(s)$, where $\mathcal{T}_{\perp,\parallel} = \mathcal{T}_{\perp,\parallel}^-$, read as [37].

$$T_1(s) = \mathcal{T}_\perp, \qquad T_2(s) = \frac{2\mathcal{E}_{K^*}}{m_B}\mathcal{T}_\perp, \qquad T_3(s) = \mathcal{T}_\perp + \mathcal{T}_\parallel, \tag{2.9}$$

where $\mathcal{E}_{K^*} = (m_B^2 + m_{K^*}^2 - s)/2m_B$ is the energy of kaon in the rest frame of $B$-meson and $\mathcal{T}_{\perp,\parallel}(s)$ are defined in Eq. (B.4) of Appendix B.

The four-fold differential decay distribution for the cascade decay $B \to K^*(\to K\pi)\ell^+\ell^-$ is completely described by the four independent kinematical variables: the three angles; $\theta_{K^*}$ is the angle between the $K$ and $B$ mesons in the rest frame of $K^*$, $\theta_\ell$ is the angle between lepton and $B$ meson in the dilepton rest frame while $\phi$ is the azimuthal angle between the dilepton rest frame and $K^*$ rest frame. The fourth variable is dilepton invariant squared mass $s$. The explicit dependence of differential decay distribution on these kinematical variables can be expressed as follows

$$\frac{d^4\Gamma}{ds\, d\cos\theta_\ell\, d\cos\theta_{K^*} d\phi} = \frac{9}{32\pi}\widetilde{\Gamma}\left(s, \theta_\ell, \theta_{K^*}, \phi\right), \tag{2.10}$$

where

$$\begin{aligned}\widetilde{\Gamma}\left(s, \theta_\ell, \theta_{K^*}, \phi\right) &= J_1^s \sin^2\theta_{K^*} + J_1^c \cos^2\theta_{K^*} + \left(J_2^s \sin^2\theta_{K^*} + J_2^c \cos^2\theta_{K^*}\right)\cos 2\theta_\ell \\ &+ J_3 \sin^2\theta_{K^*}\sin^2\theta_\ell \cos 2\phi + J_4 \sin 2\theta_{K^*}\sin 2\theta_\ell \cos\phi + J_5 \sin 2\theta_{K^*}\sin\theta_\ell\cos\phi \\ &+ (J_6^s \sin^2\theta_{K^*} + J_6^c \cos^2\theta_{K^*})\cos\theta_\ell + J_7 \sin 2\theta_{K^*}\sin\theta_\ell \sin\phi \\ &+ J_8 \sin 2\theta_{K^*}\sin 2\theta_\ell \sin\phi + J_9 \sin^2\theta_{K^*}\sin^2\theta_\ell \sin 2\phi\,. \end{aligned} \tag{2.11}$$

The full physical region phase space of kinematical variables is given by

$$4m_\ell^2 \leqslant s \leqslant (m_B - m_{K^*})^2\,, \qquad 0 \leqslant \theta_\ell \leqslant \pi, \qquad 0 \leqslant \theta_{K^*} \leqslant \pi, \qquad 0 \leqslant \phi \leqslant 2\pi, \tag{2.12}$$

where $m_B$, $m_{K^*}$, $m_\ell$ are the masses of $B$ meson, $K^*$ and lepton, respectively.

The expressions of coefficients $J_i^{(a)} = J_i^{(a)}(s)$ for $i = 1, ...., 9$ and $a = s, c$ as a function of the dilepton mass $s$, are given in Eq. (2.15). As we do not take the scalar contribution in this study, therefore, $J_6^c = 0$.

### 2.2 Expressions of the Angular Observables

The definitions of form factors independent optimal observables are given in ref. [14],

$$\begin{aligned} P_1(s) &= \frac{J_3}{2J_2^s}, \quad P_2(s) = \beta_\ell \frac{J_6^s}{8J_2^s}, \quad P_3(s) = -\frac{J_9}{4J_2^s}, \quad P_4(s) = \frac{\sqrt{2}J_4}{\sqrt{-J_2^c(2J_2^s - J_3)}}, \\ P_5(s) &= \frac{\beta_\ell J_5}{\sqrt{-2J_2^c(2J_2^s + J_3)}}, \quad P_6(s) = -\frac{\beta_\ell J_7}{\sqrt{-2J_2^c(2J_2^s - J_3)}}. \end{aligned} \tag{2.13}$$

**Table 1**. The values of the fit parameters involved in the calculations of the form factors given in Eq. (2.8) [30].

| | $r_1$ | $r_2$ | $m_R^2(\mathrm{GeV}^2)$ | $m_{fit}^2(\mathrm{GeV}^2)$ |
|---|---|---|---|---|
| $V(s)$ | 0.923 | -0.511 | 28.30 | 49.40 |
| $A_1(s)$ | | 0.290 | | 40.38 |
| $A_2(s)$ | -0.084 | 0.342 | | 52.00 |

The primed observables (related to the $P_i$ $(i = 4, 5, 6)$) which are simpler and more efficient to fit experimentally are defined as,

$$P_4' \equiv P_4\sqrt{1-P_1} = \frac{J_4}{\sqrt{-J_2^c J_2^s}}, \quad P_5' \equiv P_5\sqrt{1+P_1} = \frac{J_5}{2\sqrt{-J_2^c J_2^s}},$$
$$P_6' \equiv P_6\sqrt{1-P_1} = \frac{-J_7}{2\sqrt{-J_2^c J_2^s}}. \tag{2.14}$$

We get the following expressions of $J_i$ as follows,

$$\begin{aligned}
J_1^s &= \frac{3s\beta_\ell^2}{2}\Big[p_{K^*}^2 s\left(|g_1|^2+|h_1|^2\right)+|g_2|^2+|h_2|^2\Big]+\frac{8m_\ell^2}{s}(p_{K^*}^2 s|h_1|^2+|h_2|^2),\\
J_1^c &= \frac{2}{m_{K^*}^2}\Big[32\,\mathrm{a}_0^2\,C_{10}^{\mathrm{tot}^2} m_{K^*}^2 m_\ell^2 p_{K^*}^2+\beta_\ell^2 s|E_{K^*}g_2+2\sqrt{s}p_{K^*}^2 g_3|^2\\
&\quad+\left(2-\beta_\ell^2\right)s|E_{K^*}h_2+2\sqrt{s}p_{K^*}^2 h_3|^2\Big],\\
J_2^s &= \frac{1}{2}s\beta_\ell^2\Big[P_{K^*}^2 s\left(|g_1|^2+|h_1|^2\right)+|g_2|^2+|h_2|^2\Big],\\
J_2^c &= -\frac{2\beta_\ell^2 s}{m_{K^*}^2}\Big[|E_{K^*}\mathrm{g}_2+2\sqrt{s}p_{K^*}^2 g_3|^2+|E_{K^*}h_2+2\sqrt{s}p_{K^*}^2 h_3|^2\Big],\\
J_3 &= s\beta_\ell^2\Big[p_{K^*}^2 s\left(|g_1|^2+|h_1|^2\right)-|g_2|^2-|h_2|^2\Big],\\
J_4 &= \frac{\sqrt{2}s\beta_\ell^2}{m_{K^*}}\Big[E_{K^*}\left(|g_2|^2+|h_2|^2\right)+p_{K^*}^2\,(s)^{1/2}\,2\mathcal{R}e(g_2g_3^*+h_2h_3^*)\Big],\\
J_5 &= -\frac{\sqrt{8}p_{K^*}\,(s)^{3/2}\,\beta_\ell}{m_{K^*}}\Big[E_{K^*}\mathcal{R}e(g_1h_2^*+g_2h_1^*)+2p_{K^*}^2 s^{1/2}\mathcal{R}e(g_1h_3^*+g_3h_1^*)\Big],\\
J_6^s &= -4p_{K^*}\,(s)^{3/2}\,\beta_\ell\Big[\mathcal{R}e(g_1h_2^*+g_2h_1^*)\Big], \quad J_7 = \frac{\sqrt{32}p_{K^*}^2\,(s)^{3/2}\,\beta_\ell}{m_{K^*}}\Big[\mathcal{I}m(g_2h_3^*+g_3^*h_2)\Big],\\
J_8 &= \frac{\sqrt{2}p_{K^*}\,(s)^{3/2}\,\beta_\ell^2}{m_{K^*}}\Big[E_{K^*}\mathcal{I}m(g_1^*g_2+h_1^*h_2)+2p_{K^*}^2 s^{1/2}\mathcal{I}m(g_1^*g_3+h_1^*h_3)\Big],\\
J_9 &= 2p_{K^*}\,(s)^{3/2}\,\beta_\ell^2\Big[\mathcal{I}m(g_1g_2^*+h_2h_1^*)\Big],
\end{aligned} \tag{2.15}$$

where $g_i(h_i)$, $i = 1, \cdots, 3$ are the auxiliary functions and given as follows,

$$\begin{aligned}
h_1 &= \frac{4m_b}{s}\mathcal{T}_\perp+\frac{2}{M_B+m_{K^*}}C_9^{\mathrm{tot}}V(s), \quad g_1 = \frac{2}{M_B+m_{K^*}}C_{10}^{\mathrm{tot}}V(s),\\
h_2 &= -(M_B+m_{K^*})C_9^{\mathrm{tot}}A_1(s)-\frac{4m_b\left(m_B^2-m_{K^*}^2\right)}{s}\frac{E_{K^*}}{M_B}\mathcal{T}_\perp, \;\; g_2 = -(M_B+m_{K^*})A_1(s)C_{10}^{\mathrm{tot}},\\
h_3 &= \frac{A_2}{M_B+m_{K^*}}C_9^{\mathrm{tot}}+\frac{2m_b}{s}\left[\frac{s(\mathcal{T}_\perp+\mathcal{T}_\parallel)}{m_B^2-m_{K^*}^2}+\frac{2E_{K^*}}{M_B}\mathcal{T}_\perp\right], \quad g_3 = \frac{A_2}{M_B+m_{K^*}}C_{10}^{\mathrm{tot}},
\end{aligned} \tag{2.16}$$

$$E_{K^*} = \frac{m_B^2-m_{K^*}^2-s}{2\sqrt{s}}, \quad p_{K^*} = \sqrt{E_{K^*}^2-m_{K^*}^2}, \quad \beta_\ell = \sqrt{1-\frac{4m_\ell^2}{s}}, \tag{2.17}$$

and $a_0 = \frac{E_{K^*}}{m_{K^*}} \frac{\xi_\parallel}{\Delta_\parallel}$ where $\Delta_\parallel$ is given in Appendix B in Eq. (B.1).

Traditionally, the $J$'s are given in terms of transversity amplitudes but we have written in terms of $g_i(h_i)$ functions given in Eq. (2.16) $A_{0,\parallel,\perp}$. The $A_{0,\parallel,\perp}$ are related with $g_i(h_i)$ as follows

$$A_0^{L,R} = \frac{\mathcal{N}}{m_{K^*}}\Big[E_{k^*}(h_2 \mp g_2) + 2p_{k^*}^2\sqrt{s}(h_3 \mp g_3)\Big],$$
$$A_\parallel^{L,R} = \sqrt{2}\mathcal{N}\big[h_2 \mp g_2\big], \qquad A_\perp^{L,R} = \sqrt{2s}\mathcal{N}p_{k^*}\big[h_1 \mp g_1\big], \tag{2.18}$$

where $\mathcal{N} = \alpha\, G_F |V_{tb}V_{ts}^*| \sqrt{\frac{s\,\beta_\ell\, p_{K^*}}{3\cdot 2^{10}\pi^5 m_B^3}}$.

## 3 Results and Discussion

In this section, we will present the numerical analysis of the angular observables. Before start the analysis, in the following we would like to write the different definitions of angular observables that are opted by LHCb [4] and theoretically used in the literature,

$$P_2^{\rm exp} = -P_2, \quad P_3^{\rm exp} = -P_3, \quad P_4'^{\rm exp} = -\frac{1}{2}P_4', \quad P_6'^{\rm exp} = -P_6', \tag{3.1}$$

and $P_1^{\rm exp} = P_1$, $P_5'^{\rm exp} = P_5'$.

For the numerical values of the LCSR form factors, given in Eq. (2.8), the values of relevant fit parameters are listed in Tab. (1). The values of Wilson coefficients and the values of other parameters which we used in the numerical calculations are listed in Appendix A in Tabs. (4) and (6), respectively.

### 3.1 $P$-observables in different bin size

Our results for $P$-observables in the SM, in different $Z'$ scenarios and their comparison with maximum likelihood fit results of ref. [4] by LHCb in different bin size are summarized in Tab. (2) and graphically shown in Figs. (1) and (2) where black crosses are the data points taken from the last column of Tab. (2) and black dashed line correspond to the SM while green, red and blue bands correspond to the $\mathcal{S}_1$, $\mathcal{S}_2$ and $\mathcal{S}_3$ scenarios of the $Z'$ model, respectively. In our different bin sized analysis, we have not included the preliminary results from Belle [6, 7], ATLAS [8] and CMS[1] [9, 10] because their bin intervals are different from LHCb [4] that we have discussed in this section. The continuous plots over $s$ are presented with SM uncertainty band in light gray color. This uncertainty is mainly coming through parametric uncertainty including form factors, though these observables are FFI. Let us also explicitly mention that while performing these calculations using different form factors (e.g, [5]), it is indeed the case that these observables are form factors independent. One can see from the left panel of Figs. (1) and (2) that the uncertainty band in SM not preclude the effects of $Z'$ model. Keeping in mind this we have not provided the SM uncertainty bands for different bins in Tab. (2) and hence in the right panel of Figs. (1) and (2). However, for $s \in [1, 6]\text{GeV}^2$, we do have listed in Tab. (3) and in Fig. (3).

[1] see figure 6 of [11] for the recent analysis with these new results.

**Table 2**. Results for $\langle P \rangle$-observables and their comparison with maximum likelihood fit results of ref. [4] in different bin size.

| Obs. | SM Prediction | $\mathcal{S}_1$ | $\mathcal{S}_2$ | $\mathcal{S}_3$ | Measurement [4] |
|---|---|---|---|---|---|
| $0.1 < s < 0.98$ GeV$^2$ | | | | | |
| $\langle P_1 \rangle$ | $-0.002$ | $-0.002 \leftrightarrow -0.008$ | $-0.002 \leftrightarrow -0.002$ | $-0.002 \leftrightarrow -0.009$ | $-0.099^{+0.168}_{-0.163} \pm 0.014$ |
| $\langle P_2 \rangle$ | $-0.106$ | $-0.134 \leftrightarrow -0.113$ | $-0.116 \leftrightarrow -0.102$ | $0.042 \leftrightarrow -0.059$ | $-0.003^{+0.051}_{-0.052} \pm 0.007$ |
| $\langle P_3 \rangle$ | $-0.0001$ | $0.000 \leftrightarrow -0.0002$ | $-0.000 \leftrightarrow -0.001$ | $-0.000 \leftrightarrow -0.0001$ | $0.113^{+0.079}_{-0.079} \pm 0.006$ |
| $\langle P'_4 \rangle$ | 0.267 | $0.175 \leftrightarrow 0.155$ | $0.230 \leftrightarrow 0.171$ | $0.405 \leftrightarrow 0.380$ | $0.185^{+0.158}_{-0.154} \pm 0.023$ |
| $\langle P'_5 \rangle$ | 0.740 | $0.747 \leftrightarrow 0.473$ | $0.712 \leftrightarrow 0.497$ | $-0.209 \leftrightarrow 0.424$ | $0.387^{+0.132}_{-0.133} \pm 0.052$ |
| $\langle P'_6 \rangle$ | $-0.158$ | $-0.447 \leftrightarrow -0.585$ | $-0.384 \leftrightarrow -0.566$ | $0.466 \leftrightarrow 0.400$ | $0.034^{+0.134}_{-0.135} \pm 0.015$ |
| $1.1 < s < 2.5$ GeV$^2$ | | | | | |
| $\langle P_1 \rangle$ | $-0.007$ | $-0.008 \leftrightarrow -0.008$ | $-0.007 \leftrightarrow -0.008$ | $-0.006 \leftrightarrow -0.006$ | $-0.415^{+0.519}_{-0.636} \pm 0.038$ |
| $\langle P_2 \rangle$ | $-0.433$ | $-0.417 \leftrightarrow -0.161$ | $-0.406 \leftrightarrow -0.187$ | $0.097 \leftrightarrow -0.347$ | $-0.373^{+0.146}_{-0.199} \pm 0.027$ |
| $\langle P_3 \rangle$ | 0.0001 | $-0.000 \leftrightarrow 0.001$ | $0.000 \leftrightarrow 0.001$ | $0.001 \leftrightarrow 0.001$ | $0.350^{+0.330}_{-0.254} \pm 0.015$ |
| $\langle P'_4 \rangle$ | 0.023 | $-0.113 \leftrightarrow -0.173$ | $-0.040 \leftrightarrow -0.13$ | $0.170 \leftrightarrow 0.200$ | $-0.163^{+0.232}_{-0.240} \pm 0.021$ |
| $\langle P'_5 \rangle$ | 0.225 | $0.275 \leftrightarrow -0.208$ | $0.211 \leftrightarrow -0.141$ | $0.249 \leftrightarrow 0.160$ | $0.289^{+0.220}_{-0.202} \pm 0.023$ |
| $\langle P'_6 \rangle$ | $-0.078$ | $-0.432 \leftrightarrow -0.533$ | $-0.400 \leftrightarrow -0.536$ | $0.689 \leftrightarrow 0.520$ | $-0.463^{+0.202}_{-0.221} \pm 0.012$ |
| $2.5 < s < 4.0$ GeV$^2$ | | | | | |
| $\langle P_1 \rangle$ | -0.023 | $-0.025 \leftrightarrow -0.026$ | $-0.024 \leftrightarrow -0.025$ | $-0.032 \leftrightarrow -0.024$ | $0.571^{+2.404}_{-1.714} \pm 0.045$ |
| $\langle P_2 \rangle$ | $-0.228$ | $-0.215 \leftrightarrow 0.154$ | $-0.188 \leftrightarrow 0.110$ | $-0.341 \leftrightarrow -0.280$ | $-0.636^{+0.444}_{-1.735} \pm 0.015$ |
| $\langle P_3 \rangle$ | 0.001 | $-0.000 \leftrightarrow 0.002$ | $0.001 \leftrightarrow 0.002$ | $0.004 \leftrightarrow 0.004$ | $0.745^{+2.587}_{-0.861} \pm 0.030$ |
| $\langle P'_4 \rangle$ | $-0.282$ | $-0.355 \leftrightarrow -0.394$ | $-0.320 \leftrightarrow -0.371$ | $-0.314 \leftrightarrow -0.205$ | $-0.713^{+0.410}_{-1.305} \pm 0.024$ |
| $\langle P'_5 \rangle$ | $-0.400$ | $-0.204 \leftrightarrow -0.667$ | $-0.339 \leftrightarrow -0.628$ | $0.722 \leftrightarrow -0.294$ | $-0.066^{+0.343}_{-0.364} \pm 0.023$ |
| $\langle P'_6 \rangle$ | $-0.066$ | $-0.313 \leftrightarrow -0.350$ | $-0.309 \leftrightarrow -0.372$ | $0.568 \leftrightarrow 0.508$ | $0.205^{+0.962}_{-0.341} \pm 0.013$ |
| $4.0 < s < 6.0$ GeV$^2$ | | | | | |
| $\langle P_1 \rangle$ | -0.055 | $-0.053 \leftrightarrow -0.053$ | $-0.054 \leftrightarrow -0.053$ | $-0.064 \leftrightarrow -0.062$ | $0.180^{+0.364}_{-0.348} \pm 0.0.027$ |
| $\langle P_2 \rangle$ | 0.206 | $0.088 \leftrightarrow 0.357$ | $0.170 \leftrightarrow 0.341$ | $-0.407 \leftrightarrow 0.146$ | $0.042^{+0.088}_{-0.087} \pm 0.011$ |
| $\langle P_3 \rangle$ | 0.001 | $-0.000 \leftrightarrow 0.003$ | $0.000 \leftrightarrow 0.003$ | $0.003 \leftrightarrow 0.004$ | $0.083^{+0.187}_{-0.184} \pm 0.023$ |
| $\langle P'_4 \rangle$ | $-0.443$ | $-0.460 \leftrightarrow -0.472$ | $-0.452 \leftrightarrow -0.465$ | $-0.477 \leftrightarrow -0.446$ | $-0.448^{+0.169}_{-0.172} \pm 0.020$ |
| $\langle P'_5 \rangle$ | 0.761 | $-0.492 \leftrightarrow -0.837$ | $-0.653 \leftrightarrow -0.829$ | $0.682 \leftrightarrow -0.514$ | $-0.300^{+0.158}_{-0.159} \pm 0.023$ |
| $\langle P'_6 \rangle$ | $-0.036$ | $-0.182 \leftrightarrow -0.198$ | $-0.178 \leftrightarrow -0.214$ | $0.249 \leftrightarrow 0.268$ | $-0.032^{+0.167}_{-0.166} \pm 0.007$ |

The plots in first and third rows of Fig. (1), represent the variation in the values of $P_{1,3}$ and their average values $\langle P_{1,3} \rangle$ as a function of $s$ in the SM and in the different scenarios of $Z'$ model. From these graphs one can see that the values of these observables are quite small in the SM and not much enhanced when we incorporate the $Z'$ effects. One can also see from Fig. (1) that the SM values of $\langle P_1 \rangle$ lie inside the measured values, however with huge error bars, so no potent result can be drawn from this observable with current data. On the other hand the values of $\langle P_3 \rangle$ in last two bins are within the measured values while in first two bins the SM values are out of the measured bars. However, to say something about any discrepancy in these observables, reduction in the experimental uncertainties are required.

Plots in second row of Fig. (1), show the variation in the values of $P_2$ and its average $\langle P_2 \rangle$ against dilepton mass $s$. It could be seen from these figures that the values of these observables are significantly influenced in the presence of $Z'$ effects. The right plot in

the second row of Fig. (1) shows that the SM values of $\langle P_2 \rangle$ in the bins $s \in [1.1, 2.5]$ and $s \in [2.5, 4.0]$ lie within the measurements and also in the bin $s \in [4.0, 6, 0]$ when the theoretical uncertainties of the input parameters are taken into account. However, in the first bin $s \in [0.1, 0.98]$, the SM value of $\langle P_2 \rangle$ looks mismatch from the experimental value but it is worthy to mention here that the measurement performed by LHCb in this bin is without including the $m_\ell-$ suppressed terms which are important at very low $s$ region and it was found in [38], that the impact of these terms results is about 23% reductionn in the value of $\langle P_2 \rangle$. Regarding this, it is mentioned in [15] that in the first bin, LHCb actually measured $\langle \hat{P}_2 \rangle$ instead of $\langle P_2 \rangle$. Therefore, in principle, one could say that, up-till now, there is no mismatch between the SM predicted values of $\langle P_2 \rangle$ with the experimental values.

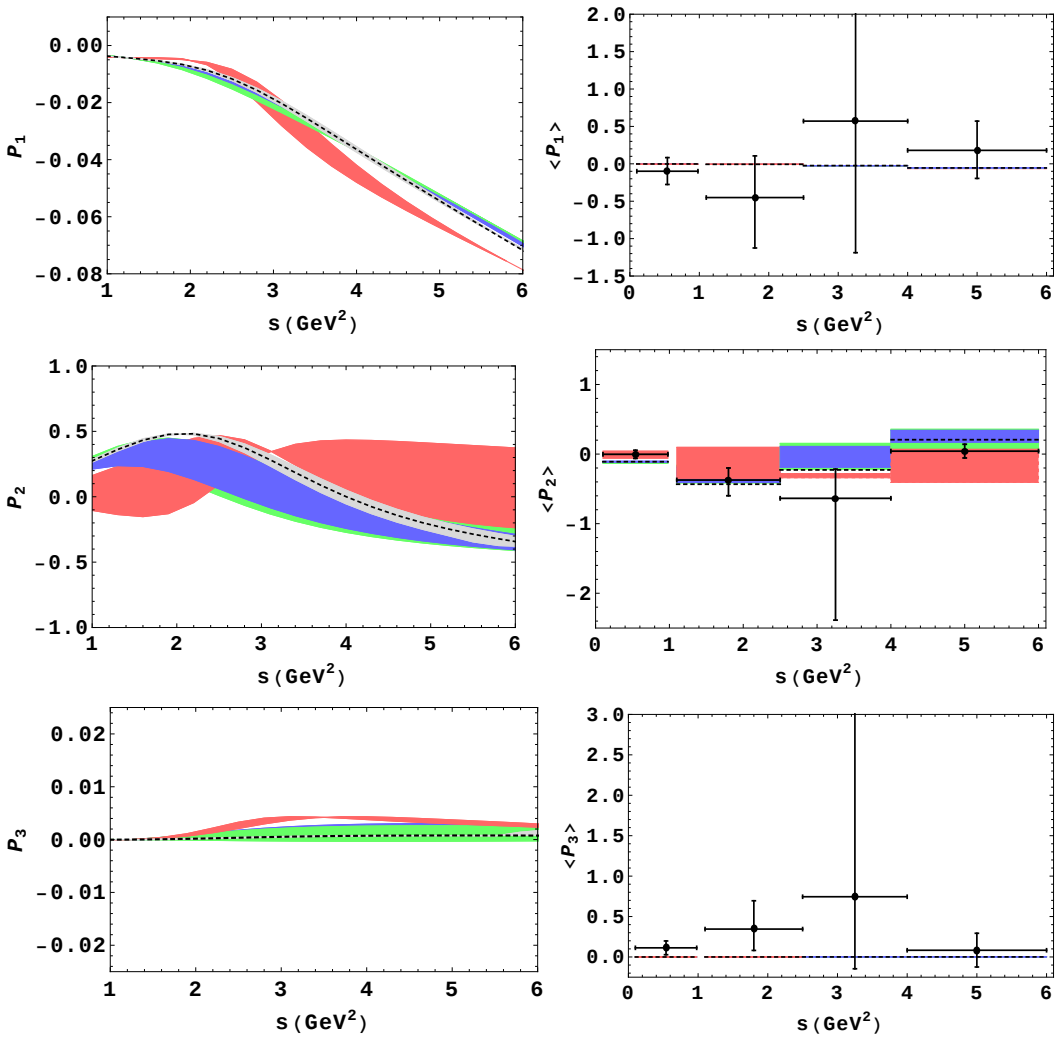


**Figure 1**. The dependence of the optimal observables, $P_{1,2,3}$ and $\langle P_{1,2,3} \rangle$ for the decay $B \to K^*(\to K\pi) l^+ l^-$ on $s$. The black dashed line correspond to the SM while green, blue and red bands correspond to the $\mathcal{S}_1$, $\mathcal{S}_2$ and $\mathcal{S}_3$ scenarios of the $Z'$ model, respectively.

In the first row plots of Fig. (2), we have displayed $P_4'$ and it's average value $\langle P_4' \rangle$ in the SM and in the different scenarios of $Z'$ model as a function of $s$. One can see from these plots that the $Z'$ effects are quite significant in the $P_4'$ values at low $s$ region but mild at larger values of $s$. However, the SM values of $\langle \mathcal{P}_4' \rangle$ in all four bins lie inside the experimentally measured values.

The results of $P_5'$ and it's average value $\langle P_5' \rangle$ in the SM and in the $Z'$ models are presented in the second row plots of Figs. (2). The values are significantly changed from the SM values when we incorporate the $Z'$ effects. It can be noticed in the bin $s = 4$ to 6 GeV$^2$, the SM average value $\langle P_5' \rangle$ mismatch with the experimental values and as mentioned in the introduction that LHCb found $2.6\sigma$ deviation in this bin. Regarding this discrepancy, our analysis shows that the average value $\langle P_5' \rangle$ in this bin could be adjusted with the measured value by using $\mathcal{S}_3$ parametric space of $Z'$ model, as shown in right plot of second row of Fig. (2) by red band.

In the third row plots of Fig. (2), we have shown the variation of $P_6'$ and $\langle P_6' \rangle$ as a function of $s$. Similar to $P_{1,3}$, the SM value of this observable is also suppressed. As seen from the graph that SM value of $P_6'$ consistent with the data with large error bars, however there is $2\sigma$ deviation in one bin $s \in [1.1, 2.5]$ which probably will be disappear when data will increase. On the NP point of view, in contrast to the $P_{1,3}$, the value of $P_6'$ significantly enhanced in the $Z'$ model. It is also noticed that in the $Z'$ model the value of $P_6'$ is positive in scenarios $\mathcal{S}_1$ and $\mathcal{S}_2$ while becomes negative in $\mathcal{S}_3$ .

### 3.2 $P$-observables in $s \in [1.0, 6.0]$ GeV$^2$

The results for $P$-observables in $s \in [1.0, 6.0]$ GeV$^2$ are summarized in Tab. (3) and corresponding plots are shown in Fig. (3) where, magenta [6] and yellow [7] error bars correspond to available Belle measurements for some of these observables. It is worth to mention that LHCb results [4] are for $s \in [1.1, 6.0]$ GeV$^2$ whereas, both Belle measurements [6, 7] are for $s \in [1.0, 6.0]$ GeV$^2$. Moreover, recently the ATLAS collaboration [8] announced its results for $s \in [0.04, 6.0]$ GeV$^2$ that we have not include in our analysis. The empty red box in $\langle P_2 \rangle$ and $\langle P_6' \rangle$ represents the $\mathcal{S}_3$ scenario when we choose $\phi_{sb} = -150 \pm 10$ given in Appendix A, while, other legends are same as in Figs. (1) and (2).

From Fig. (3), one can notice immediately that the values of $\langle P_1 \rangle$ and $\langle P_4' \rangle$ in the SM and in all the three scenarios of $Z'$ lie within the current measurements. It is also noticed that the values of $\langle P_1 \rangle$ in the SM and in the $Z'$ scenarios are very close, consequently, this observable even after the reduction of error bars not a good candidate to constrained the $Z'$ parametric space. On the other hand $\langle P_4' \rangle$ could be helpful to constrained the $Z'$ parametric space, if any mismatch will appear in future in the bin [1,6] GeV$^2$. The $\langle P_3 \rangle$ has small values in the SM and in all the three scenarios of considered model while measured value is well above the prediction, however, more data is required to cast any result from this observable. In the plots of $\langle P_2 \rangle$ and $\langle P_6' \rangle$, one can deduced that the SM value of $\langle P_2 \rangle$ not lie within the measured error bars while the SM value of $\langle P_6' \rangle$ lie within the measurements, however for both observables, values in $\mathcal{S}_1$ and $\mathcal{S}_2$ lie also within the measurements while the values in $\mathcal{S}_3$ lie outside the measured values (see red bands in both figures). Regarding $\mathcal{S}_3$, it is interesting to check whether the value in this scenario could be

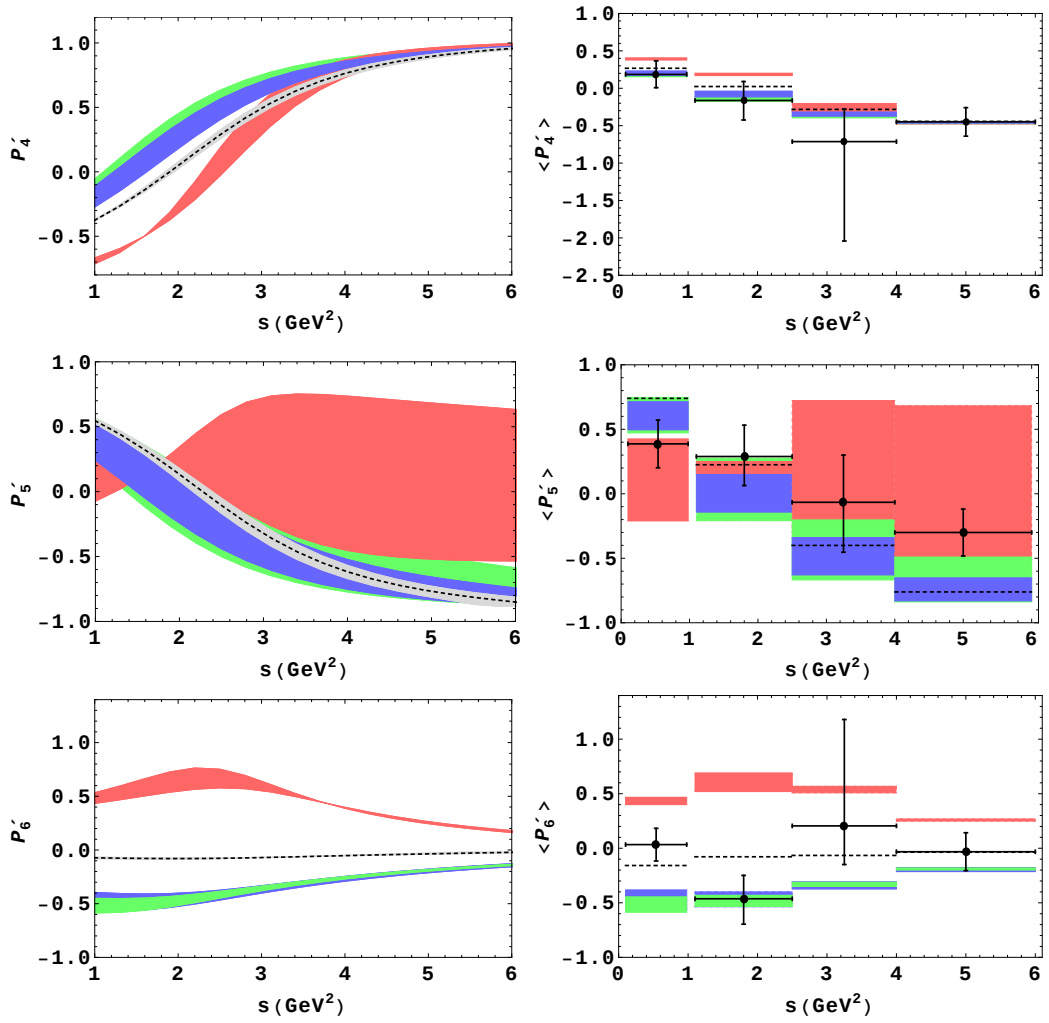


**Figure 2**. The dependence of the optimal observables, $P'_{4,5,6}$ and $\langle P'_{4,5,6}\rangle$ for the decay $B \to K^*(\to K\pi)l^+l^-$ on $s$, the legends are same as in Fig. (1).

reduced to accommodate with current measurement, for this purpose, we choose $\mathcal{S}_3$ with the opposite sign of $\phi_{sb}$ angle i.e, given in the parenthesis of Tab. 5 in Appendix A. This is indeed the case as one can see from the empty red boxes in these two plots. In $\langle P_2\rangle$ the empty red box is close to measurements as compare to red band. Similarly, in $\langle P'_6\rangle$ red box is within the Belle measurements [6]. Therefore, more statistics on the observables $\langle P_2\rangle$ and $\langle P'_6\rangle$ are helpful to constrained the $Z'$ parameters, particularly, the sign and the magnitude of new weak phase $\phi_{sb}$.

For $\langle P'_5\rangle$ plots of Fig. (3), the values in the SM and in $\mathcal{S}_1$, $\mathcal{S}_2$ lie out side the error basrs of experimental data points while the values in the $\mathcal{S}_3$ well inside the all data points shown in figure. In general, from the plots of Fig. (3), one concludes that the considered model do have potential to remove mismatch between theory and experiment but it is not so conclusive at present. We hope more precise measurements will clear the situation.

**Table 3**. Results for $\langle P \rangle$-observables for $s \in [1.0, 6.0]$ GeV$^2$ and their comparison with LHCb maximum likelihood fit results of ref. [4] in different bin size, Belle results [6, 7].

| Obs. | SM Prediction | $\mathcal{S}_1$ | $\mathcal{S}_2$ | $\mathcal{S}_3$ | Measurement |
|---|---|---|---|---|---|
| $\langle P_1 \rangle$ | -0.033±0.001 | $-0.032 \leftrightarrow -0.034$ | $-0.033 \leftrightarrow -0.033$ | $-0.039 \leftrightarrow -0.036$ | $0.080^{+0.248}_{-0.245} \pm 0.044$ [4] |
| $\langle P_2 \rangle$ | $0.091 \pm 0.033$ | $0.133 \leftrightarrow -0.162$ | $0.087 \leftrightarrow -0.135$ | $0.254 \leftrightarrow 0.106$ | $-0.162^{+0.072}_{-0.073} \pm 0.010$ [4] |
| $\langle P_3 \rangle$ | $0.001 \pm 0.000$ | $-0.000 \leftrightarrow 0.002$ | $0.000 \leftrightarrow 0.002$ | $0.003 \leftrightarrow 0.003$ | $0.205^{+0.135}_{-0.134} \pm 0.017$ [4] |
| $\langle P_4' \rangle$ | $-0.264 \pm 0.014$ | $-0.333 \leftrightarrow -0.368$ | $-0.298 \leftrightarrow -0.347$ | $-0.195 \leftrightarrow -0.256$ | $-0.336^{+0.124}_{-0.122} \pm 0.12$ [4]<br>$-0.095^{+0.302}_{-0.309} \pm 0.174$ [6]<br>$-0.22^{+0.35}_{-0.34} \pm 0.15$ [7] |
| $\langle P_5' \rangle$ | $-0.378 \pm 0.051$ | $-0.197 \leftrightarrow -0.617$ | $-0.322 \leftrightarrow -0.583$ | $0.572 \leftrightarrow -0.260$ | $-0.049^{+0.107}_{-0.108} \pm 0.014$ [4]<br>$0.385^{+0.276}_{-0.285} \pm 0.099$ [6]<br>$0.43^{+0.26}_{-0.28} \pm 0.10$ [7] |
| $\langle P_6' \rangle$ | $-0.056 \pm -0.000$ | $-0.287 \leftrightarrow -0.330$ | $-0.276 \leftrightarrow -0.345$ | $0.452 \leftrightarrow 0.403$ | $-0.166^{+0.108}_{-0.108} \pm 0.021$ [4]<br>$-0.202^{+0.278}_{-0.270} \pm 0.172$ [6] |

### 3.3 $Q_{4,5}$ for $s \in [1.0, 6.0]$ GeV$^2$

In Fig. (4), we have plotted the lepton flavor universality violation (LFUV) observables $\langle Q_{4(5)} \rangle$ against $s$. The values are quite small in the SM approximately $\langle Q_{4(5)} \rangle = 8.8 \pm 2.1 \times 10^{-3} (7.5 \pm 3.6 \times 10^{-3})$ in the bin $s \in [1, 6]$GeV$^2$. We have also found that the effects of $Z'$ are very mild, consequently, there is no enhancement in the values of these observable. However, error bars are quite large and need more experimental data to find the accurate values of these observables.

## 4 Conclusion

In the present study, we have calculated the FFI observables $P_i$ and their average values $\langle P_i \rangle$ in the SM and in the $Z'$ model for $B \to K^*(\to K\pi)\ell^+\ell^-$. The expressions of these observables are given in the form of $J_i(s)$ which are written in terms of auxiliary functions $g_i(h_i)$ in Eq. (2.15). These coefficients, in general, expressed via transversity amplitudes that are $A_\perp$, $A_\parallel$ and $A_0$, the relations of these transversity amplitudes with $g_i(h_i)$ are given in Eq. (2.18). To see the $Z'$ effects, we use the UtFit collaboration constraints for the $Z'$ parameters. It is found that the values of these angular observables are significantly changed from their SM values in the presence of $Z'$, particularly, at small values of $s$, i.e the large recoil region. We have also found that the SM values of some of the observables under consideration, in some bins of $s$, are mismatch with the recent experimental result and the $Z'$ parametric space has potential to accommodate these mismatch. For instance, there is a discrepancy between experimentally measured value and SM value of $P_5'$ in the region $s \in [4, 6]$ GeV$^2$ and in the current study it is found that scenario $\mathcal{S}_3$ of $Z'$ could be adjust this mismatch value with the measured value in this bin. Furthermore, we have also calculated the angular observables $\langle P_i \rangle$ and the LFUV observables $\langle Q_{4,5} \rangle$ in the large bin $s \in [1, 6]$ and plotted with the measured data, however, the error bar is quite large in this bin and more static is needed to draw results. Here, we would like to comment that CMS and ATLAS collaborations recently announced preliminary results on angular observables

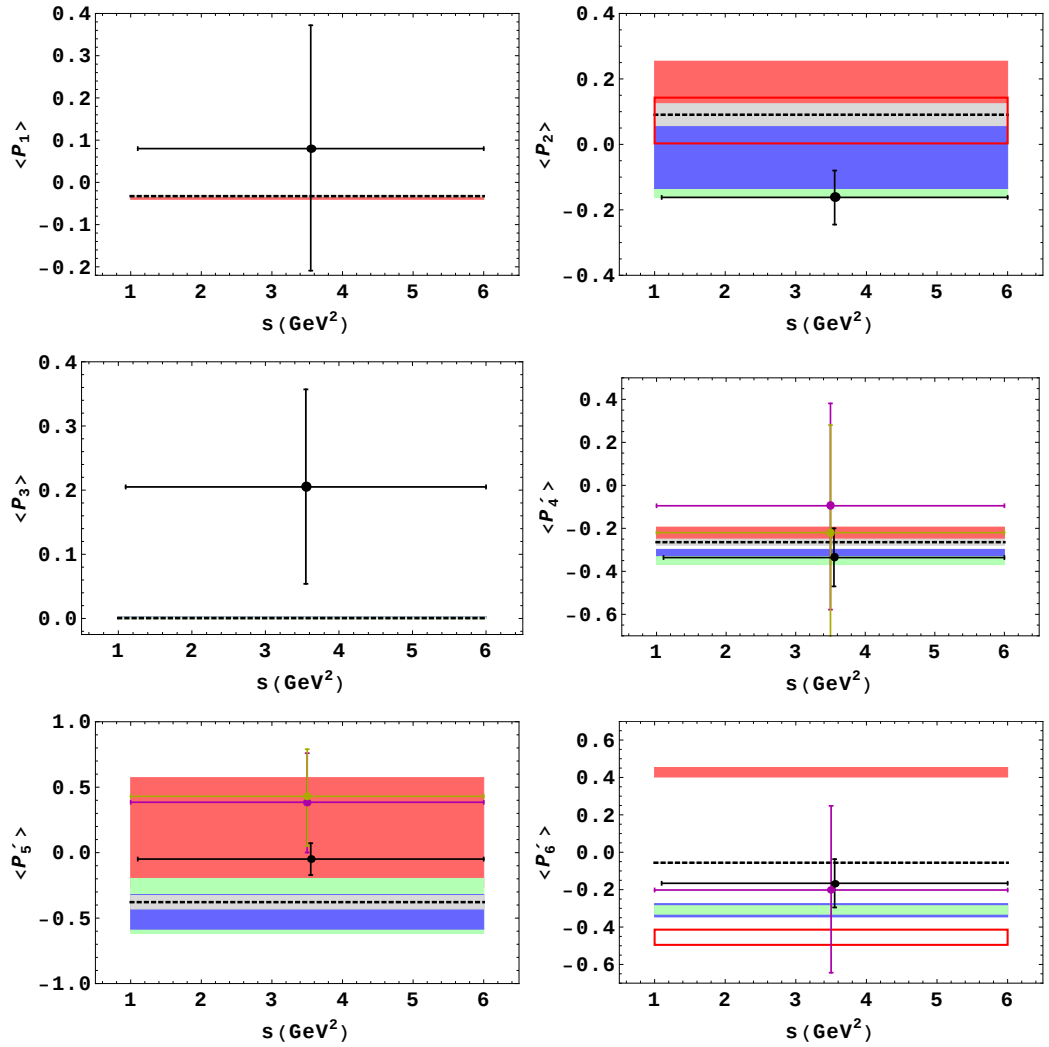


**Figure 3**. Optimal observables for $s \in [1.0, 6.0]$ GeV$^2$ where, magenta [6] and yellow [7] error bars correspond to Belle measurements available for some of these observables. The empty red box in $\langle P_2 \rangle$ and $\langle P_6' \rangle$ represents the $\mathcal{S}_3$ when we choose $\phi_{sb} = -150 \pm 10$ given in Tab. 5 of Appendix A. Other legends are same as in Figs. (1) and (2).

in Moriond 2017 which still show the tension between experimental measurements and the SM predictions. Therefore, in general, one can say, as data will be enlarge and the statistical error will be reduced then these observables are quite promising to say something about the constraints on coupling of $Z'$ boson with the quarks and leptons and consequently about the status of $Z'$ model.

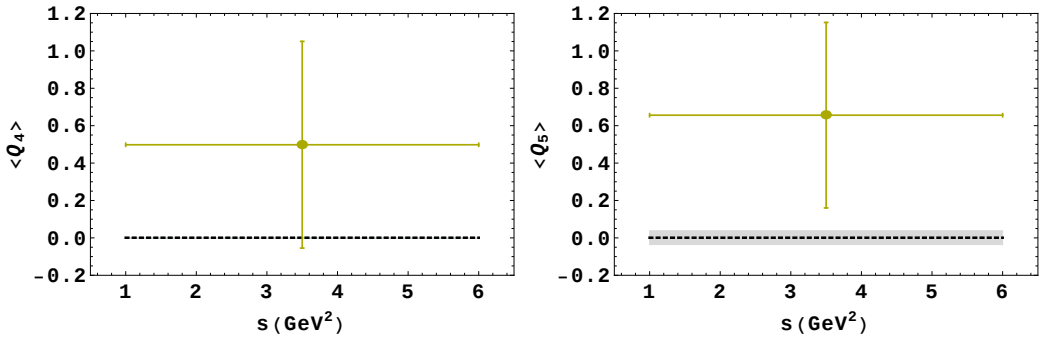


**Figure 4**. Optimal observables $Q_4$, $Q_5$ for $s \in [1.00, 6.00]$ GeV$^2$ where, yellow error bar corresponds to recent Belle measurements [7]. Other legends are same as in previous figures.

## A Input parameters

The values of Wilson coefficients at NNLO, $Z'$ parameters and other input parameters are listed in Tabs. (4), (5) and (6), respectively.

**Table 4**. Values of Wilson coefficients at $\mu_b = 4 \cdot 8$.

| $C_1(\mu_b)$ | $C_2(\mu_b)$ | $C_3(\mu_b)$ | $C_4(\mu_b)$ | $C_5(\mu_b)$ | $C_6(\mu_b)$ | $C_7^{\rm eff}(\mu_b)$ | $C_8^{\rm eff}(\mu_b)$ | $C_9(\mu_b)$ | $C_{10}(\mu_b)$ |
|---|---|---|---|---|---|---|---|---|---|
| -0.2632 | 1.0111 | -0.0055 | -0.0806 | 0.0004 | 0.0009 | -0.2923 | -0.1663 | 4.0749 | -4.3085 |

**Table 5**. The numerical values of the $Z'$ parameters [39–41].

| | $\lvert\mathcal{B}_{sb}\rvert \times 10^{-3}$ | $\phi_{sb}$(Degree) | $S_{LL} \times 10^{-2}$ | $D_{LL} \times 10^{-2}$ |
|---|---|---|---|---|
| $\mathcal{S}1$ | $1.09 \pm 0.22$ | $-72 \pm 7$ | $-2.8 \pm 3.9$ | $-6.7 \pm 2.6$ |
| $\mathcal{S}2$ | $2.20 \pm 0.15$ | $-82 \pm 4$ | $-1.2 \pm 1.4$ | $-2.5 \pm 0.9$ |
| $\mathcal{S}3$ | $4.0 \pm 1.5$ | $150 \pm 10$ or $(-150 \pm 10)$ | 0.8 | $-2.6$ |

## B NLO contributions in the low dilepton mass limit

The expression of $\Delta_\parallel$, appear in the definition of $a_0$ below Eq. (2.17), written as follows

$$\Delta_\parallel(s) = 1 + \frac{\alpha_s C_F}{4\pi}\left[(2L-2) - \frac{2s}{E_{K^*}^2}\frac{\pi^2 f_B f_{K^*\parallel}\lambda_{B+}^{-1}}{N_c m_B (E_{K^*}/m_{K^*})\xi_\parallel(s)}\int_0^1 \frac{du}{\bar{u}}\Phi_{\bar{K}^*,\parallel}\right], \tag{B.1}$$

and contributes only for massive leptons. The light-cone distribution amplitude (LCDA) $\Phi_{\bar{K}^*,a}$ for transversely ($a = \perp$) and longitudinally ($a = \parallel$) polarized $K^*$ can be written as [37, 43]

$$\Phi_{\bar{K}^*,a} = 6u(1-u)\left\{1 + a_1\left(\bar{K}^*\right)_a C_1^{(3/2)}(2u-1) + a_2\left(\bar{K}^*\right)_a C_2^{(3/2)}(2u-1)\right\}, \tag{B.2}$$

**Table 6**. Values of input parameters.

| | | | |
|---|---|---|---|
| $\alpha_{em}(M_Z) = 1/128.940$ | [47] | $\alpha_s(M_Z) = 0.1184 \pm 0.0007$ | [48] |
| $m_e = 0.51099 \times 10^{-3}$ GeV | [48] | $m_\mu = 0.10565837$ GeV | [48] |
| $m_B = 5.27950$ GeV | [48] | $m_{K^*} = 0.89594$ GeV | [48] |
| $m_b^{1S} = 4.68 \pm 0.03$ GeV | [49] | $m_s = 0.095 \pm 0.005$ GeV | [48] |
| $m_c^{\overline{MS}}(m_c) = 1.27 \pm 0.09$ GeV | [48] | | |
| $\lvert V_{tb}\rvert = 0.999139 \pm 0.000045$ | [48] | $\lvert V_{ts}\rvert = (40.5 \pm 0.11) \cdot 10^{-3}$ | [48] |
| $f_B = 194 \pm 10$ MeV | [52] | $\lambda_B = 460 \pm 110$ MeV | [51] |
| $f_{K^*,\lVert} = 220 \pm 5$ MeV | [50] | $f_{K^*,\perp} = 185 \pm 9$ MeV | [50] |
| $a_{1,\lVert} = 0.03 \pm 0.03$ | [30] | $a_{2,\lVert} = 0.08 \pm 0.06$ | [30] |
| $a_{1,\perp} = 0.03 \pm 0.03$ | [30] | $a_{2,\perp} = 0.08 \pm 0.06$ | [30] |

where $L = -(m_b^2 - s)/s \ln\left(1 - s/m_b^2\right)$ and $a_i\left(\bar{K}^*\right)_a$ are the Gegenbauer coefficients. The moments are

$$\lambda_{B,+}^{-1} = \int_0^\infty d\omega \frac{\Phi_{B,+}(\omega)}{\omega} , \quad \text{and} \quad \lambda_{B,-}^{-1} = \int_0^\infty d\omega \frac{\Phi_{B,-}(\omega)}{\omega - s/m_B - i\epsilon}$$

where $\Phi_{B,\pm}$ are the two $B$-meson light-cone distribution amplitudes [37]. The $\lambda_{B,-}^{-1}(s)$ can be expressed as:

$$\lambda_{B,-}^{-1}(s) = \frac{e^{-s/(m_B\omega_0)}}{\omega_0}\left[-\mathbf{Ei}\left(s/m_B\omega_0\right) + i\pi\right],$$

where $\omega_0 = 2(m_B - m_b)$. The $\xi_a$ are the universal form factors,

$$\xi_\perp = \frac{m_B}{m_B + m_{K^*}} V , \quad \text{and} \quad \xi_\lVert = \frac{m_B + m_{K^*}}{2E_{K^*}} A1 - \frac{m_B - m_{K^*}}{m_B} A2. \tag{B.3}$$

The $B \to K^*$ matrix elements in heavy quark limit depend on four independent functions $\mathcal{T}_a^\pm$ ($a = \perp, \lVert$). In the low $s$, ($1.0 < s < 6.0\,\text{GeV}^2$), the invariant amplitudes $\mathcal{T}_{\perp,\lVert}$ at NLO within QCDf are given in [35, 37, 42],

$$\mathcal{T}_a = \xi_a C_a + \frac{\pi^2}{N_c}\frac{f_B f_{K^*,a}}{m_B}\Xi_a \sum_\pm \int \frac{d\omega}{\omega}\Phi_{B,\pm}(\omega)\int_0^1 du \Phi_{K^*,a}(u)\, T_{a,\pm}(u,\omega) , \tag{B.4}$$

where $\Xi_\perp \equiv 1$, $\Xi_\lVert \equiv m_{K^*}/E_{K^*}$ and the factorization scale $\mu_f = \sqrt{m_b \Lambda_{QCD}}$. The coefficient functions $C_a$ and hard scattering functions $T_{a,\pm}$ are written as

$$C_a = C_a^{(0)} + \frac{\alpha_s(\mu_b) C_F}{4\pi} C_a^{(1)} , \quad \text{and} \quad T_{a,\pm} = T_{a,\pm}^{(0)}(u,\omega) + \frac{\alpha_s(\mu_f) C_F}{4\pi} T_{a,\pm}^{(1)}(u,\omega) . \tag{B.5}$$

The form factor terms $C_a^{(0)}$ at LO are

$$C_\perp^{(0)} = C_7^{\text{eff}} + \frac{s}{2m_b m_B} Y(s) , \quad \text{and} \quad C_\lVert^{(0)} = -C_7^{\text{eff}} - \frac{m_B}{2m_b} Y(s) .$$

$$Y(s) = h(s,m_c)\left(\frac{4}{3}C_1 + C_2 + 6C_3 + 60C_5\right) - \frac{1}{2}h(s,m_b^{\rm pole})\left(7C_3 + \frac{4}{3}C_4 + 76C_5 + \frac{64}{3}C_6\right)$$
$$- \frac{1}{2}h(s,0)\left(C_3 + \frac{4}{3}C_4 + 16C_5 + \frac{64}{3}C_6\right) + \frac{4}{3}C_4 + \frac{64}{9}C_5 + \frac{64}{27}C_6,$$

where $h(s,m_q)$ is well-known fermionic loop function.
The coefficients $C_a^{(1)}$ at NLO is divided into a factorizable and a non-factorizable part as

$$C_a^{(1)} = C_a^{(f)} + C_a^{(nf)} \,. \tag{B.6}$$

At NLO the factorizable correction reads [37, 44]

$$C_\perp^{(f)} = C_7^{\rm eff}\left(\ln\frac{m_b^2}{\mu^2} - L + \Delta M\right) \,, \qquad \text{and} \qquad C_\parallel^{(f)} = -C_7^{\rm eff}\left(\ln\frac{m_b^2}{\mu^2} + 2L + \Delta M\right).$$

The non-factorizable corrections are,

$$C_F C_\perp^{(nf)} = -\bar{C}_2 F_2^{(7)} - C_8^{\rm eff} F_8^{(7)} - \frac{s}{2m_b m_B}\left[\bar{C}_2 F_2^{(9)} + 2\bar{C}_1\left(F_1^{(9)} + \frac{1}{6}F_2^{(9)}\right) + C_8^{\rm eff} F_8^{(9)}\right],$$
$$C_F C_\parallel^{(nf)} = \bar{C}_2 F_2^{(7)} + C_8^{\rm eff} F_8^{(7)} + \frac{m_B}{2m_b}\left[\bar{C}_2 F_2^{(9)} + 2\bar{C}_1\left(F_1^{(9)} + \frac{1}{6}F_2^{(9)}\right) + C_8^{\rm eff} F_8^{(9)}\right],$$

where $\Delta M$ depends on the mass renormalization convention for $m_b$. These corrections are obtained from the matrix elements of four-quark and chromomagnetic dipole operators [37] that are embedded in $F_{1,2}^{(7,9)}$ and $F_8^{(7,9)}$ [45, 46].
At LO the hard-spectator scattering term $T_{a,\pm}^{(0)}(u,\omega)$ from weak annihilation diagram is [37]

$$T_{\perp,+}^{(0)}(u,\omega) = T_{\perp,-}^{(0)}(u,\omega) = T_{\parallel,+}^{(0)}(u,\omega) = 0 \,,$$
$$T_{\parallel,-}^{(0)}(u,\omega) = -e_q \frac{m_B\omega}{m_B\omega - s - i\epsilon}\frac{4m_B}{m_b}\left(\bar{C}_3 + 3\bar{C}_4\right) \,.$$

The contributions to $T_a^{(1)}$ at NLO also contain a factorisable as well as non-factorizable part

$$T_a^{(1)} = T_a^{(f)} + T_a^{(nf)} \,. \tag{B.7}$$

Including $\mathcal{O}(\alpha_s)$ corrections the factorizable term to $T_{a,\pm}^{(1)}$ are given by [37, 44]

$$T_{\perp,+}^{(f)}(u,\omega) = C_7^{\rm eff}\frac{2m_B}{\bar{u}E_{K^*}} \,, \quad T_{\parallel,+}^{(f)}(u,\omega) = C_7^{\rm eff}\frac{4m_B}{\bar{u}E_{K^*}} \,, \quad \text{and} \quad T_{\perp,-}^{(f)}(u,\omega) = T_{\parallel,-}^{(f)}(u,\omega) = 0 \,,$$

where $\bar{u} = 1 - u$. The non-factorizable correction comes through the matrix elements of

four-quark operators and the chromomagnetic dipole operator

$$
\begin{aligned}
T_{\perp,+}^{(nf)}(u,\omega) &= -\frac{4e_d C_8^{\text{eff}}}{u+\bar{u}s/m_B^2} + \frac{m_B}{2m_b}[e_u t_\perp(u,m_c)\left(\bar{C}_2+\bar{C}_4-\bar{C}_6\right) \\
&\quad + e_d t_\perp(u,m_b)\left(\bar{C}_3+\bar{C}_4-\bar{C}_6-4m_b/m_B\bar{C}_5\right)+e_d t_\perp(u,0)\,\bar{C}_3]\,, \\
T_{\perp,-}^{(nf)}(u,\omega) &= 0\,, \\
T_{\parallel,+}^{(nf)}(u,\omega) &= \frac{m_B}{m_b}[e_u t_\parallel(u,m_c)\left(\bar{C}_2+\bar{C}_4-\bar{C}_6\right)+e_d t_\parallel(u,m_b)\left(\bar{C}_3+\bar{C}_4-\bar{C}_6\right)+e_d t_\parallel(u,0)\,\bar{C}_3]\,, \\
T_{\parallel,-}^{(nf)}(u,\omega) &= e_q\frac{m_B\omega}{m_B\omega-s-i\epsilon}\Bigg[\frac{8C_8^{\text{eff}}}{\bar{u}+us/m_B^2}+\frac{6m_B}{m_b}\Bigg(h\left(\bar{u}m_B^2+us,m_c\right)\left(\bar{C}_2+\bar{C}_4+\bar{C}_6\right) \\
&\quad + h\left(\bar{u}m_B^2+us,m_b^{pole}\right)\left(\bar{C}_3+\bar{C}_4+\bar{C}_6\right)+h\left(\bar{u}m_B^2+us,0\right)\left(\bar{C}_3+3\bar{C}_4+3\bar{C}_6\right) \\
&\quad - \frac{8}{27}\left(\bar{C}_3-\bar{C}_5-15\bar{C}_6\right)\Bigg)\Bigg].
\end{aligned}
$$

The $t_a(u,m_q)$ functions are given by

$$
\begin{aligned}
t_\perp(u,m_q) &= \frac{2m_B}{\bar{u}E_{K^*}}I_1(m_q)+\frac{s}{\bar{u}^2E_{K^*}^2}\left(B_0\left(\bar{u}m_B^2+us,m_q\right)-B_0(s,m_q)\right), \\
t_\parallel(u,m_q) &= \frac{2m_B}{\bar{u}E_{K^*}}I_1(m_q)+\frac{\bar{u}m_B^2+us}{\bar{u}^2E_{K^*}^2}\left(B_0\left(\bar{u}m_B^2+us,m_q\right)-B_0(s,m_q)\right)\,,
\end{aligned}
$$

where $B_0$ and $I_1$ are

$$
B_0(s,m_q) = -2\sqrt{4m_q^2/s-1}\arctan\frac{1}{\sqrt{4m_q^2/s-1}}\,,
$$

$$
I_1(m_q) = 1+\frac{2m_q^2}{\bar{u}\left(m_B^2-s\right)}\left[L_1(x_+)+L_1(x_-)-L_1(y_+)-L_1(y_-)\right]\,,
$$

and

$$
x_\pm = \frac{1}{2}\pm\left(\frac{1}{4}-\frac{m_q^2}{\bar{u}m_B^2+us}\right)^{1/2}, \qquad y_\pm = \frac{1}{2}\pm\left(\frac{1}{4}-\frac{m_q^2}{s}\right)^{1/2}\,,
$$

$$
L_1(x) = \ln\frac{x-1}{x}\ln(1-x)-\frac{\pi^2}{6}+Li_2\left(\frac{x}{x-1}\right).
$$

## References


[1] S. Descotes-Genon, J. Matias, M. Ramon and J. Virto, JHEP **1301**, 048 (2013) doi:10.1007/JHEP01(2013)048 [arXiv:1207.2753 [hep-ph]].

[2] S. Descotes-Genon, T. Hurth, J. Matias and J. Virto, "Optimizing the basis of $B \to K*ll$ observables in the full kinematic range," JHEP **1305**, 137 (2013), [arXiv:1303.5794 [hep-ph]].

[3] **LHCb** Collaboration, "Measurement of Form-Factor-Independent Observables in the Decay $B^0 \to K^{*0}\mu^+\mu^-$," PRL **111** (2013) 191801 [arXiv:1308.1707 [hep-ex]].

[4] R. Aaij *et al.* [LHCb Collaboration], "Angular analysis of the $B^0 \to K^{*0}\mu^+\mu^-$ decay using 3 $\text{fb}^{-1}$ of integrated luminosity," JHEP **1602** (2016) 104 [arXiv:1512.04442 [hep-ex]].

[5] A. Bharucha, D. M. Straub and R. Zwicky, JHEP **1608**, 098 (2016) doi:10.1007/JHEP08(2016)098 [arXiv:1503.05534 [hep-ph]].

[6] A. Abdesselam *et al.* [Belle Collaboration], "Angular analysis of $B^0 \to K^*(892)^0\ell^+\ell^-$," arXiv:1604.04042 [hep-ex].

[7] S. Wehle *et al.* [Belle Collaboration], "Lepton-Flavor-Dependent Angular Analysis of $B \to K^*\ell^+\ell^-$," arXiv:1612.05014 [hep-ex].

[8] **ATLAS** Collaboration, *Angular analysis of* $B_d^0 \to K^*\mu^+\mu^-$ *decays in pp collisions at* $\sqrt{s} = 8$ *TeV with the ATLAS detector*, Tech. Rep. ATLAS-CONF-2017-023, CERN, Geneva, 2017.

[9] **CMS** Collaboration, *Measurement of the* $P_1$ *and* $P_5'$ *angular parameters of the decay* $\text{B}^0 \to \text{K}^{*0}\mu^+\mu^-$ *in proton-proton collisions at* $\sqrt{s} = 8$ TeV, Tech. Rep. CMS-PAS-BPH-15-008, CERN, Geneva, 2017.

[10] **CMS** Collaboration, V. Khachatryan et al., *Angular analysis of the decay* $B^0 \to K^{*0}\mu^+\mu^-$ *from pp collisions at* $\sqrt{s} = 8$ *TeV*, *Phys. Lett.* **B753** (2016) 424–448, [arXiv:1507.08126].

[11] W. Altmannshofer, C. Niehoff, P. Stangl and D. M. Straub, "Status of the $B \to K^*\mu^+\mu^-$ anomaly after Moriond 2017," arXiv:1703.09189 [hep-ph].

[12] **LHCb** Collaboration, "Test of lepton universality using $B^+ \to K^+\ell^+\ell^-$ decays," Phys. Rev. Lett. **113** (2014) 151601 [arXiv:1406.6482 [hep-ex]].

[13] R. Aaij *et al.* [LHCb Collaboration], "Angular analysis and differential branching fraction of the decay $B_s^0 \to \phi\mu^+\mu^-$," JHEP **1509** (2015) 179 [arXiv:1506.08777 [hep-ex]].

[14] J. Matias, F. Mescia, M. Ramon and J. Virto, "Complete Anatomy of $\bar{B}_d \to \bar{K}^{*0}(\to K\pi)\ell^+\ell^-$ and its angular distribution," JHEP **1204** (2012) 104, arXiv:1202.4266 [hep-ph], and references therein.

[15] B. Capdevila, S. Descotes-Genon, L. Hofer and J. Matias, "Hadronic uncertainties in $B \to K^*\mu^+\mu^-$: a state-of-the-art analysis," arXiv:1701.08672 [hep-ph].

[16] V. G. Chobanova, T. Hurth, F. Mahmoudi, D. Martinez Santos and S. Neshatpour, "Large hadronic power corrections or new physics in the rare decay $B \to K^*\mu^+\mu^-$?," arXiv:1702.02234 [hep-ph].

[17] S. Descotes-Genon, J. Matias and J. Virto, Phys. Rev. D **88**, 074002 (2013) [arXiv:1307.5683 [hep-ph]]; W. Altmannshofer and D. M. Straub, Eur. Phys. J. C **73** (2013) 2646] [arXiv:1308.1501 [hep-ph]]; T. Hurth and F. Mahmoudi, JHEP **1404** (2014) 097 [arXiv:1312.5267 [hep-ph]]; F. Mahmoudi, S. Neshatpour and J. Virto, Eur. Phys. J. C **74** (2014) 6, 2927 [arXiv:1401.2145 [hep-ph]]; T. Hurth, F. Mahmoudi and S. Neshatpour, JHEP **1412** (2014) 053 [arXiv:1410.4545 [hep-ph]]; S. Jager and J. Martin Camalich, JHEP **1305** (2013) 043 [arXiv:1212.2263 [hep-ph]]; G. Hiller and M. Schmaltz, Phys. Rev. D **90** (2014) 054014 [arXiv:1408.1627 [hep-ph]]; A. J. Buras, F. De Fazio and J. Girrbach, JHEP **1402** (2014) 112 [arXiv:1311.6729 [hep-ph]]; A. J. Buras, F. De Fazio and J. Girrbach-Noe, JHEP **1408** (2014) 039 [arXiv:1405.3850 [hep-ph]]; R. Gauld, F. Goertz and U. Haisch, JHEP **1401** (2014) 069 [arXiv:1310.1082 [hep-ph]]; R. Gauld, F. Goertz and U. Haisch, Phys. Rev. D **89** (2014) 015005 [arXiv:1308.1959 [hep-ph]]; E. Lunghi and J. Matias, JHEP **0704** (2007) 058 [hep-ph/0612166]; D. Aristizabal Sierra, F. Staub and A. Vicente, Phys. Rev. D **92**, no. 1, 015001 (2015) [arXiv:1503.06077 [hep-ph]].

[18] U. Egede, T. Hurth, J. Matias, M. Ramon and W. Reece, "New physics reach of the decay mode $\bar{B} \to \bar{K}^{*0}\ell^+\ell^-$," JHEP **1010**, 056 (2010) [arXiv:1005.0571 [hep-ph]].

[19] W. Altmannshofer and D. M. Straub, "New physics in $b \to s$ transitions after LHC run 1," Eur. Phys. J. C **75**, no. 8, 382 (2015) [arXiv:1411.3161 [hep-ph]].

[20] F. Beaujean, C. Bobeth and D. van Dyk, "Comprehensive Bayesian analysis of rare (semi)leptonic and radiative $B$ decays," Eur. Phys. J. C **74**, 2897 (2014) Erratum: [Eur. Phys. J. C **74**, 3179 (2014)] [arXiv:1310.2478 [hep-ph]].

[21] T. Hurth and F. Mahmoudi, "On the LHCb anomaly in B $\to K^*\ell^+\ell^-$," JHEP **1404**, 097 (2014) [arXiv:1312.5267 [hep-ph]]; T. Hurth and F. Mahmoudi, "Signs for new physics in the recent LHCb data?," Nucl. Part. Phys. Proc. **263-264**, 38 (2015) [arXiv:1411.2786 [hep-ph]].

[22] S. Jger and J. Martin Camalich, "Reassessing the discovery potential of the $B \to K^*\ell^+\ell^-$ decays in the large-recoil region: SM challenges and BSM opportunities," Phys. Rev. D **93**, no. 1, 014028 (2016) [arXiv:1412.3183 [hep-ph]].

[23] S. Descotes-Genon, J. Matias and J. Virto, "Understanding the $B \to K^*\mu^+\mu^-$ Anomaly," Phys. Rev. D **88** (2013) 074002 [arXiv:1307.5683 [hep-ph]].

[24] W. Altmannshofer and D. M. Straub, "New physics in $B \to K^*\mu\mu$?," Eur. Phys. J. C **73** (2013) 2646 [arXiv:1308.1501 [hep-ph]].

[25] R. Gauld, F. Goertz and U. Haisch, "On minimal Z' explanations of the B-¿K*mu+mu- anomaly," Phys. Rev. D **89** (2014) 015005 [arXiv:1308.1959 [hep-ph]].

[26] R. Gauld, F. Goertz and U. Haisch, "An explicit Z'-boson explanation of the $B \to K^*\mu^+\mu^-$ anomaly," JHEP **1401** (2014) 069 [arXiv:1310.1082 [hep-ph]].

[27] A. J. Buras, F. De Fazio and J. Girrbach, "331 models facing new $b \to s\mu^+\mu^-$ data," JHEP **1402** (2014) 112 [arXiv:1311.6729 [hep-ph]].

[28] A. J. Buras and J. Girrbach, "Left-handed Z' and Z FCNC quark couplings facing new $b \to s\mu^+\mu^-$ data," JHEP **1312** (2013) 009 [arXiv:1309.2466 [hep-ph]].

[29] B. Capdevila, S. Descotes-Genon, J. Matias and J. Virto, "Assessing lepton- flavour non-universality from $B \to K^*\ell\ell$ angular analyses," JHEP **1610**, 075 (2016) [arXiv:1605.03156 [hep-ph]].

[30] P. Ball and R. Zwicky, $B_{d,s} \to \rho, \omega, K^*, \phi$ *decay form-factors from light-cone sum rules revisited*, Phys. Rev. D **71** (2005) 014029 [hep-ph/0412079].

[31] P. Langacker and M. Plumacher, "Flavor changing effects in theories with a heavy $Z'$ boson with family nonuniversal couplings," Phys. Rev. D **62**, 013006 (2000) [hep-ph/0001204].

[32] Q. Chang and Y. H. Gao, Nucl. Phys. B **845**, 179 (2011) [arXiv:1101.1272 [hep-ph]]; Y. Li, J. Hua and K. C. Yang, Eur. Phys. J. C **71**, 1775 (2011) [arXiv:1107.0630 [hep-ph]].

[33] K. Cheung, C. W. Chiang, N. G. Deshpande and J. Jiang, Phys. Lett. B **652**, 285 (2007) [hep-ph/0604223]; C. H. Chen and H. Hatanaka, Phys. Rev. D **73**, 075003 (2006) [hep-ph/0602140]; C. W. Chiang, N. G. Deshpande and J. Jiang, JHEP **0608**, 075 (2006) [hep-ph/0606122].

[34] V. Barger, C. W. Chiang, P. Langacker and H. S. Lee, Phys. Lett. B **580**, 186 (2004) [hep-ph/0310073]; V. Barger, L. Everett, J. Jiang, P. Langacker, T. Liu and C. Wagner, Phys. Rev. D **80**, 055008 (2009) [arXiv:0902.4507 [hep-ph]]; R. Mohanta and A. K. Giri,

Phys. Rev. D **79**, 057902 (2009) [arXiv:0812.1842 [hep-ph]]; J. Hua, C. S. Kim and Y. Li, Eur. Phys. J. C **69**, 139 (2010) [arXiv:1002.2531 [hep-ph]].

[35] C. Bobeth, G. Hiller and G. Piranishvili, "CP Asymmetries in bar $B \to \bar{K}^*(\to \bar{K}\pi)\bar{\ell}\ell$ and Untagged $\bar{B}_s$, $B_s \to \phi(\to K^+K^-)\bar{\ell}\ell$ Decays at NLO," JHEP **0807**, 106 (2008) [arXiv:0805.2525 [hep-ph]].

[36] M. Beneke and T. Feldmann, "Symmetry breaking corrections to heavy to light B meson form-factors at large recoil," Nucl. Phys. B **592**, 3 (2001) [hep-ph/0008255].

[37] M. Beneke, T. Feldmann and D. Seidel, "Systematic approach to exclusive $B \to Vl^+l^-$, $V\gamma$ decays," Nucl. Phys. B **612**, 25 (2001) [hep-ph/0106067].

[38] S. Descotes-Genon, L. Hofer, J. Matias and J. Virto, "Global analysis of $b \to s\ell\ell$ anomalies," JHEP **1606**, 092 (2016) [arXiv:1510.04239 [hep-ph]].

[39] Q. Chang, X. Q. Li and Y. D. Yang, JHEP **1002** (2010) 082 [arXiv:0907.4408] [hep-ph]

[40] M. Bona et al., (UTfit collaboration), PMC Phys. a **3** (2009) [arXiv:0803.0659 [hep-ph]]; M. Bona et al., arXiv: 0906.0953 [hep-ph]; C. -H. Chen, Phys. Lett. B 683 (2010) 160 [arXiv:0911.3479 [hep-ph]]; N. G. Deshpande, X.-G. He and G. Valencia, Phys. Rev. D 82(2010) 056013 [arXiv:1006.1682 [hep-ph]]; J. E. Kim, M. -S. Seo and S. Shin, Phys. Rev. D 83 (2011) 036003 [arXiv:1010.5123 [hep-ph]]; P. J. Fox, J. Liu, D. Tucker-Smith and N. Weiner, Phys. Rev. D 84 (2011) 115006 [arXiv:1104.4127 [hep-ph]]; Q. Chang, R. -M. Wang, Y. -G. Xu and X. -W. Cui, Chin. Phys. Lett. 28(2011) 081301.

[41] V. Barger, C. -W. Chiang, J. Jiang and P. Langacker, Phys. Lett. B 596(2004) 229 [hep-ph/0405108]; K. Cheung, C. -W.Chiang, N. G. Deshpande and J. Jiang, Phys. Lett. B 652(2007) 285 [hep-ph/0604223]; X. -G. He and G. Valencia,Phys.Rev. D 74(2006) 013011 [hep-ph/0605202]; S. Baek, J. H. Jeon and C. S. Kim, Phys. Lett. B 664 (2008) 84 [arXiv:0803.0062 [hep-ph]]; S. Sahoo, C. K. Das and L. Maharana, Int. J. Mod. Phys. A 26 (2011) 3347 [arXiv:1112.0460 [hep-ph]].

[42] W. Altmannshofer, P. Ball, A. Bharucha, A. J. Buras, D. M. Straub and M. Wick, "Symmetries and Asymmetries of $B \to K^*\mu^+\mu^-$ Decays in the Standard Model and Beyond," JHEP **0901**, 019 (2009) [arXiv:0811.1214 [hep-ph]].

[43] P. Ball and M. Boglione, "SU(3) breaking in K and K* distribution amplitudes," Phys. Rev. D **68**, 094006 (2003) [hep-ph/0307337].

[44] M. Beneke, T. Feldmann and D. Seidel, "Exclusive radiative and electroweak $b \to d$ and $b \to s$ penguin decays at NLO," Eur. Phys. J. C **41**, 173 (2005) [hep-ph/0412400].

[45] H. H. Asatryan, H. M. Asatrian, C. Greub and M. Walker, Phys. Rev. D **65**, 074004 (2002) [hep-ph/0109140]; H. H. Asatrian, H. M. Asatrian, C. Greub and M. Walker, Phys. Lett. B **507**, 162 (2001) [hep-ph/0103087].

[46] C. Greub, V. Pilipp and C. Schupbach, "Analytic calculation of two-loop QCD corrections to $b \to sl^+l^-$ in the high $q^2$ region," JHEP **0812**, 040 (2008) [arXiv:0810.4077 [hep-ph]].

[47] M. Misiak *et al.*, "Estimate of $\mathcal{B}(\bar{B} \to X_s\gamma)$ at $\mathcal{O}(\alpha_s^2)$," Phys. Rev. Lett. **98**, 022002 (2007) [hep-ph/0609232].

[48] K. A. Olive *et al.* (Particle Data Group), "Review of Particle Physics", Chin. Phys. C38, 090001 (2014).

[49] C. W. Bauer, Z. Ligeti, M. Luke, A. V. Manohar and M. Trott, "Global analysis of inclusive B decays," Phys. Rev. D **70**, 094017 (2004) [hep-ph/0408002].

[50] P. Ball, G. W. Jones and R. Zwicky, "$B \to V\gamma$ beyond QCD factorisation," Phys. Rev. D **75**, 054004 (2007) [hep-ph/0612081].

[51] P. Ball and R. Zwicky, "$|V_{td}/V_{ts}|$ from $B \to V\gamma$," JHEP **0604**, 046 (2006) [hep-ph/0603232].

[52] F. Mahmoudi, S. Neshatpour and J. Orloff, "Supersymmetric constraints from $B_s \to \mu^+\mu^-$ and $B \to K * \mu^+\mu^-$ observables," JHEP **1208**, 092 (2012) [arXiv:1205.1845 [hep-ph]].